Optics Letters

Direct soliton generation in microresonators

Chengying Bao,[1,*] Yi Xuan,[1,2] Jose A. Jaramillo-Villegas,[1,3] Daniel E. Leaird,[1] Minghao Qi,[1,2] and Andrew M. Weiner[1,2]

[1]School of Electrical and Computer Engineering, Purdue University, 465 Northwestern Avenue, West Lafayette, Indiana 47907, USA
[2]Birck Nanotechnology Center, Purdue University, 1205 West State Street, West Lafayette, Indiana 47907, USA
[3]Facultad de Ingenierías, Universidad Tecnológica de Pereira, Pereira, RI 66003, Colombia
*Corresponding author: bao33@purdue.edu

Received 31 March 2017; revised 26 May 2017; accepted 26 May 2017; posted 30 May 2017 (Doc. ID 291763); published 23 June 2017

We investigate, numerically and experimentally, the effect of thermo-optical (TO) chaos on soliton generation dynamics in microresonators. Numerical simulations that include the thermal dynamics show that the generated solitons can either survive or annihilate when the pump laser is scanned from blue to red and then stop at a fixed wavelength; the outcome is stochastic and is strongly related to the number of solitons generated. The random fluctuations of the cavity resonance occurring under TO chaos are also found to trigger delayed spontaneous soliton generation after the laser scan ends, which could enable soliton excitation with slow laser tuning speed. Stochastic soliton annihilation/survival, as well as delayed spontaneous soliton generation, is observed experimentally in a silicon-nitride microresonator.

OCIS codes: (190.5530) Pulse propagation and temporal solitons; (190.4390) Nonlinear optics, integrated optics.

https://doi.org/10.1364/OL.42.002519

Chaos is a fundamental phenomenon that widely exists in physics. In Kerr comb generation in optical microresonators [1,2], nonlinear dynamics can also lead to chaos [3,4]. The chaotic fluctuation of the intracavity power associated with this optical chaos can result in thermal chaos via the optical (TO) effect, which shifts the cavity resonance and the pump frequency detuning stochastically. Since the comb properties are sensitive to pump frequency detuning [4–6], thermal chaos will act back on the optical chaos. Here, we refer this interplay between optical chaos and thermal chaos as TO chaos.

The influence of TO chaos is especially important for the soliton Kerr comb generation, as the transition from the chaotic state to the soliton state is accompanied by a significant drop in the intracavity power, which strongly blueshifts the cavity resonance [4,7]. This blueshift could cause the pump to fall out of resonance. Hence, the soliton generation exhibits a transient instability in microresonators with a strong thermal effect such as silicon-nitride (SiN) and silica (SiO_2) cavities [7–9]. To mitigate the transient instability, complicated experimental methods such as "power-kicking" [7,10] and backward tuning [8,11,12] are usually needed. The "power-kicking" method needs additional devices (acousto-optic modulators or electro-optic modulators). The backward tuning method is limited by the response time of lasers or heaters and only works for samples exhibiting a soliton-step of long duration. For full integration of the comb system and out-of-lab applications, it is better to avoid the additional devices and complicated experimental methods. Hence, direct soliton generation (DSG), which we define as simply tuning the laser from the blue to the red and stopping at a specific wavelength to excite the soliton, is highly desired. DSG was first demonstrated in MgF_2 whispering gallery mode cavities [4], and it benefits from the low TO coefficient of MgF_2. DSG is also possible in Si microresonators, but assistance from multi-photon absorption and free carrier absorption are needed [13]. DSG has also been demonstrated in chip-scale SiN microresonators [10,11,14]. However, the important role of TO chaos was not discussed, and interesting generation phenomena related to the TO chaos were not unveiled. Since SiN has low loss in the telecom band and is compatible with CMOS integration, an understanding of DSG in SiN microresonators is critical for the integration of soliton Kerr combs, which could greatly shrink the footprint of light sources for optical communications [15], spectroscopy [16], arbitrary optical waveform generation, [17] etc.

In this Letter, we investigate DSG in SiN microresonators numerically and experimentally. In addition, we show two phenomena in DSG: (1) a new regime where solitons generated during identical laser scans in different experimental trials can either remain (survive) or annihilate, subsequent to the end of the scan, depending on the number of solitons initially generated (we refer to this as "stochastic soliton annihilation/survival"); (2) delayed spontaneous soliton generation from a chaotic state after the end of the laser scan. By modeling the soliton generation in SiN microresonators using the generalized Lugiato–Lefever equation (LLE) [18,19], supplemented by the thermal dynamics [11], we numerically predict the stochastic soliton annihilation/survival in DSG. The presence of TO chaos also allows various routes to soliton formation, including a spontaneous soliton generation route where, after a delay, the Kerr comb transits to the soliton state spontaneously after the laser scan ends (while the laser frequency is held constant). These two numerical predicted phenomena associated with

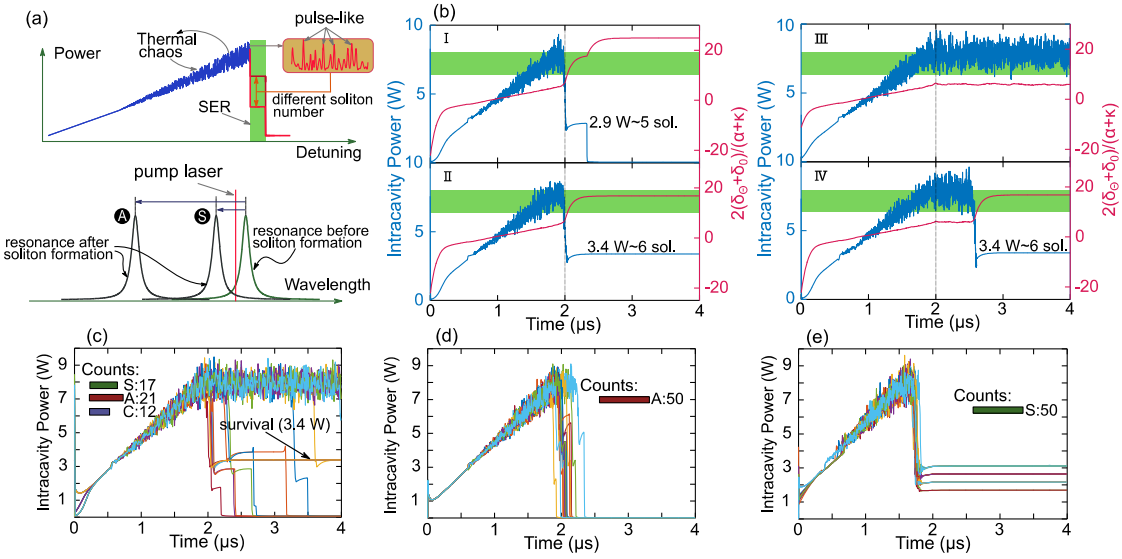

Fig. 1. DSG schematic and simulations. (a) TO chaos and its effect on DSG. How closely the pulse-like structures in the chaotic waveform (shown in the shaded box) are to the sech-shape of soliton can affect how many solitons are generated and the power drop upon soliton formation. Depending on the thermal shift associated with the power drop in the soliton generation, the system can exhibit stochastic soliton annihilation/survival. SER, soliton existence range. (b) Various routes to soliton generation in DSG: solitons can form around the end of the laser scan and (I) annihilate or (II) survive; when solitons survive, Δ_{eff} stays in the SER (illustrated by the green box), which is mapped to be $9.2 < \Delta_{\text{eff}} < 17.9$ with the thermal effect turned off. The comb can remain chaotic when the laser scan ends (III, IV). When the laser frequency is held constant, the comb can (III) remain in the chaotic regime or (IV) form solitons spontaneously. Power change in 50 scans (only 20 power traces are plotted for clarity) under (c) intermediate thermal effects, $\xi = -4.5 \times 10^4$ $(\text{Ws})^{-1}$; note that the results for several distinct trials with a soliton survival overlap closely and are hard to distinguish. (d) Strong thermal effects $\xi = -1.2 \times 10^5$ $(\text{Ws})^{-1}$ and (e) weak thermal effects, $\xi = -1.2 \times 10^4$ $(\text{Ws})^{-1}$. Under intermediate thermal effects, both soliton annihilation and survival are observed. S, survival; A, annihilation; C, chaotic.

DSG are observed experimentally in a SiN microresonator. Furthermore, we achieve soliton generation in SiN microresonators with a minute-scale laser tuning speed, orders of magnitude slower than previous demonstrations [10–12,14].

In Kerr comb generation, solitons only exist in a narrow range of detuning [11,19], which we refer to as the soliton existence range (SER) [Fig. 1(a)]. Moreover, the characteristics of the waveform in the chaotic state will affect how many pulse-like structures can develop into solitons. The intracavity power drops and the corresponding cavity resonance blueshifts that occur with transition from chaotic to soliton states depend on the power prior to soliton formation and the number of solitons generated and will differ in repeated trials. In some cases, the pump frequency detuning stays within the SER, resulting in soliton survival in DSG while, in the other cases, detuning is shifted out of the SER, resulting in soliton annihilation, as illustrated in Fig. 1(a).

To analyze the soliton generation dynamics quantitatively, we start our investigation of the soliton generation with a numerical simulation based on the generalized LLE [18,19], including thermal effects [11]. Thermal effects have been modeled in simulations of soliton number control by backward tuning of the laser after the generation and stabilization of a multi-soliton state [11]. Here, we use this model to study the dynamics of DSG. In simulations, thermal effects will have an additional pump phase detuning in the LLE, and we write the generalized LLE as [11,19]

$$\left(t_R\frac{\partial}{\partial t}+\frac{\alpha+\kappa}{2}+i\frac{\beta_2 L}{2}\frac{\partial^2}{\partial\tau^2}+i(\delta_0+\delta_\Theta)\right)E-\sqrt{\kappa}E_{in}$$
$$-i\gamma\left(1+\frac{i}{\omega_0}\right)L\left(E\int_{-\infty}^{+\infty}R(\tau')|E(t,\tau-\tau')|^2\mathrm{d}\tau'\right)=0, \quad (1)$$

$$\frac{d\delta_\Theta}{dt}=-\frac{\delta_\Theta}{\tau_0}+\xi P. \quad (2)$$

Here, E, t_R, L, ω_0, β_2, γ, E_{in}, α, and κ are the envelopes of the intracavity field, round-trip time, cavity length, carrier frequency, group-velocity dispersion, nonlinear coefficient, pump amplitude, and intrinsic and coupling loss, respectively; $R(\tau)$ is the nonlinear response, including the instantaneous electronic and delayed Raman response (see Ref. [19] for its calculation method); $\delta_0 = (\omega_{r0} - \omega_p)t_R$ is the laser detuning (ω_{r0} is the cold cavity resonance, ω_p is the pump frequency), and $\delta_\Theta = (\omega_{r\Theta} - \omega_{r0})t_R$ is the thermal detuning. ($\omega_{r\Theta}$ is the cavity resonance shifted by thermal effects, but not by the Kerr effect.) The thermal dynamics is included in Eq. (2), where P is the average intracavity power, and ξ is the coefficient describing the shift of the detuning in response to the average intracavity power (P), which depends on the thermos-optical coefficient of the material and the absorbed power converted to heat and is chosen as -4.5×10^4 $(\text{Ws})^{-1}$ in simulations; τ_0 is the thermal response time, which was measured to be submicrosecond in our fabricated microresonators previously [20]. Note that τ_0 also depends on the design of the cavity, and we set it to be 100 ns to resemble common resonators, we choose parameters as $\alpha + \kappa = 0.0037$, $\kappa|E_{in}|^2 = 0.11$ mW, $\beta_2 = -61$ ps^2/km, $\gamma = 1.4$ $(\text{Wm})^{-1}$, and $L = 628$ μm. For brevity, we denote and normalize the laser detuning, thermal detuning, and effective detuning as $\Delta_0 = 2\delta_0/(\alpha+\kappa)$, $\Delta_\Theta = 2\delta_\Theta/(\alpha+\kappa)$, and $\Delta_{\text{eff}} = 2(\delta_0+\delta_\Theta)/(\alpha+\kappa)$, respectively.

The simulation starts from noise, and we tune Δ_0 linearly from −3 to 25 in 0–2 μs and hold it at 25 in 2–4 μs to trigger

soliton formation. For the chosen ξ, various soliton generation dynamics exist. In Fig. 1(b) I, the Kerr comb starts to form into solitons around the end of the laser tuning. With the power drop (drop to 2.9 W corresponding to five solitons) in the soliton transition, thermal detuning increases (becomes less negative) and Δ_{eff} increases, exceeding the SER, which is indicated by the green shaded boxes in Fig. 1(b). The SER for the used pump power is $9.2 < \Delta_{\text{eff}} < 17.9$, which is mapped out by scanning Δ_0 from −3 to 25 without thermal effects. Consequently, solitons annihilate due to thermal-induced resonance blueshift. In contrast, in some other scans, Δ_{eff} remains in the SER after the soliton transition (power drop to 3.4 W corresponding to six solitons), and the solitons survive in DSG [Fig. 1(b) II]. Furthermore, the presence of TO chaos also allows distinct routes to soliton formation. For instance, in some scans the comb remains in the chaotic state with a blue-detuned pump over the full 4 μs simulation [Fig. 1(b) III]. However, the transition to the soliton can happen spontaneously; even the comb remains in a chaotic state for a finite time after the laser scan stops [Fig. 1(b) IV]. The spontaneous soliton generation can be attributed to TO chaos. The intracavity power changes stochastically in the chaotic state; if the power drops to some level (Δ_Θ becomes less negative) and Δ_{eff} increases to approach the SER, soliton formation is triggered.

We now examine the stochastic soliton annihilation/survival process through 50 simulation scans in Fig. 1(c). The annihilation or survival of solitons is strongly correlated with the final intracavity power. For all the cases of soliton survival, the final powers are the same, and the soliton number is always 6. This is because a certain level of final intracavity power is needed to have a final Δ_Θ to hold Δ_{eff} in the SER. If the soliton number is too large or too small, the final Δ_Θ cannot support Δ_{eff} in the SER, and the solitons annihilate. Thus, the soliton number is constrained, and thermal effects constitute a mechanism to select an appropriate soliton number from the random nature of the initially generated solitons. Since the soliton number depends on the waveform of the chaotic state, TO chaos plays a critical role in the stochastic soliton annihilation/survival process.

Stochastic soliton annihilation/survival only occurs over a certain range of the thermal strength parameter. For instance, solitons tend to annihilate in all the scans under stronger thermal effects with $\xi = -1.2 \times 10^5$ $(\text{Ws})^{-1}$ [Fig. 1(d)]. With larger ξ, Δ_0 should end at a larger value to induce soliton transition (tuned from −3 to 57 and held at 57), thus requiring a large soliton number (high final power) to hold Δ_{eff} in the SER for soliton survival. The final intracavity power and soliton number needed in order to have soliton survival can be deduced in the following way. When the cavity reaches a steady state, $d\delta_\Theta/dt = 0$. This leads to $\delta_\Theta = \xi P \tau_0$. In order to have Δ_{eff} in the SER, we should have

$$\Delta_{\min} < 2\xi P\tau_0/(\alpha + \kappa) + \Delta_0 < \Delta_{\max}, \tag{3}$$

where $\Delta_{\min(\max)}$ is the lower (upper) boundary of the SER, i.e., $\Delta_{\min} = 7.9$, $\Delta_{\max} = 19.2$ for the used pump power. Following Eq. (3), the final power should be $6.0\ \text{W} < P < 7.4\ \text{W}$, with $\Delta_0 = 57$, $\xi = -1.2 \times 10^5$ $(\text{Ws})^{-1}$. This power requires the soliton number to be 11, 12, or 13. Although the soliton number is stochastic, it follows some distribution [11], and the needed soliton number is not accessed, thus resulting in the soliton annihilation in Fig. 1(d). For weak thermal effects, e.g., $\xi = -1.2 \times 10^4$ $(\text{Ws})^{-1}$, Δ_0 is tuned from −3 to 14 and held at 14 to induce soliton transition, and solitons survive in all the 50 scans [Fig. 1(e)]. Moreover, the soliton number is random, as soliton number will not affect Δ_{eff} significantly for weak thermal effects. Indeed, the soliton number from 1 to 13 can support soliton survival with $\Delta_0 = 14$, $\xi = -1.2 \times 10^4$ $(\text{Ws})^{-1}$.

In experiments, we test DSG in a SiN microresonator, with a loaded Q-factor of 1.4×10^6, geometry of 800 × 2000 nm, 100 μm radius, and dispersion of −60 ps^2/km. The tuning of the laser is calibrated by a wavemeter with ∼20 MHz resolution, well below the linewidth of the pumped resonance (180 MHz). Hence, the laser scan starts and stops at the same wavelength for different scans (Δ_0 is tuned in the same way). The converted comb power (blocking the pump by a notch filter) is measured by a power meter during the laser scan. Since acquiring data from wavemeters and power meters takes ∼10 ms, tuning of the laser is much slower than in simulations. However, we find that the slower tuning still captures the general dynamics of DSG. Moreover, the existence of spontaneous soliton generation suggests that the laser tuning speed is not so important in soliton generation.

We first map out the soliton-step of the studied cavity and choose a wavelength around the middle of the step as the stop wavelength under the on-chip pump power of 200 mW. Then, we tune the laser to the stop wavelength and hold at the stop wavelength to demonstrate DSG. Here, the pump laser is tuned from 1551.0141 to (and held at) 1551.0301 nm. Soliton Kerr combs are generated successfully; the cavity generally supports multiple solitons, with a representative spectrum shown in Fig. 2(a). The spectrum is structured with the center frequency shifted to the red of the pump due to Raman effects (soliton self-frequency shift), which is evidence of soliton operation, as other states do not exhibit this shift [9,19,21]. After the solitons stabilize, we can get the single-soliton state, with a smooth sech^2-like spectrum [Fig. 2(b)], by backward tuning the laser [11]. By measuring the power change during backward tuning, a soliton number can be deduced [11]. The comb in Fig. 2(a) is found to consist of five solitons. Note that we achieve soliton generation in SiN microresonators by tuning the laser over about a minute time scale, whereas tens of milliseconds or a shorter tuning time is usually used in previous experiments [7,10–12,14].

We then run 50 laser scans (scan to the stop wavelength and hold for ∼10 s) and record the power evolution to observe both the stochastic soliton annihilation/survival process and delayed spontaneous soliton generation. In Figs. 3(a)–3(d), we show various routes to soliton generation in DSG. In some scans, the transition to solitons can happen before the scan ends [Figs. 3(a) and 3(b)]. However, the comb can also be chaotic when the laser scan stops [Figs. 3(c) and 3(d)]. If the comb is chaotic, the comb may switch to a soliton state spontaneously

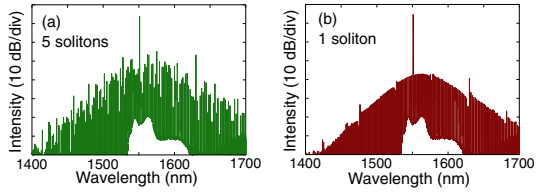

Fig. 2. Experimentally measured spectra of the solitons generated in DSG. (a) Multi-solitons and (b) single soliton.

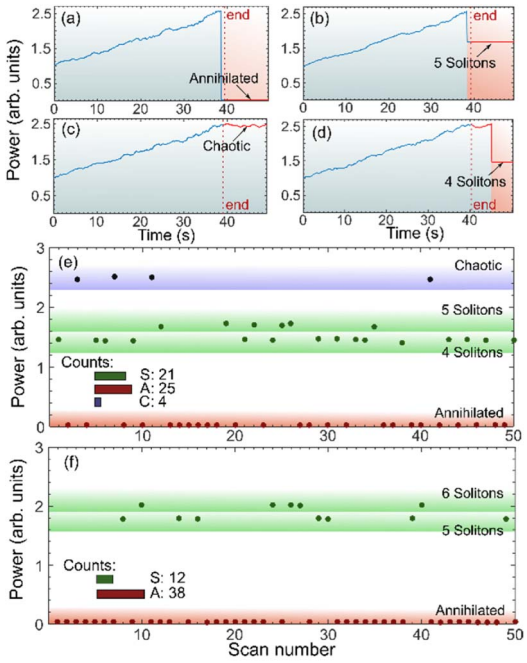

Fig. 3. Experiments exploring the generation dynamics of DSG: (a) solitons form before the laser scan ends and annihilate; (b) soliton forms before the laser scan ends and survive; (c) comb remains chaotic, with no formation of a soliton; (d) comb remains chaotic when the laser scan ends, and a soliton forms spontaneously. The dashed lines in (a)–(d) show the moments when the laser scan ends; the blue lines are the power traces recorded before the laser scan ends, while the red lines show the power traces after the laser scan ends; the blue and red shaded regions show that the laser is effective blue-detuned (chaotic) or red-tuned (soliton formed) relative to the hot cavity resonance. (e) Final intracavity power 10 s after the laser scan ends. The power levels show the operation states of the final comb, including (C) chaotic, (A) soliton annihilation, and (S) survival. (f) Final intracavity power when using a higher pump power and larger laser detuning. The soliton number tends to be larger.

in some cases after the scan stops [Fig. 3(d)]. From Figs. 3(a)–3(d), we can also see stochastic soliton annihilation/survival. For further illustration, we show the final power after holding 10 s in Fig. 3(e), which clearly shows soliton annihilation and soliton survival in different trials. Furthermore, the fraction of soliton survival and annihilation outcomes are comparable. Moreover, we also see the power restriction in the soliton survival state, as simulations predict; the soliton number is limited to four and five. We also note that DSG is not restricted to a very specific pump power and stopping wavelength. For instance, DSG can be achieved under larger laser detuning (stop at 1551.0333 nm) and higher pump power (300 mW). In this case, the soliton number tends to be larger (five or six) for soliton survival [Fig. 3(f)]. This is because the intracavity power before soliton formation becomes higher with a stronger pump; Δ_Θ is more negative prior to soliton formation. Thus, Δ_0 should be tuned to a larger value to approach the SER and induce soliton transition. To avoid a strong intracavity power drop upon soliton formation and balance the larger laser detuning (Δ_0) to hold Δ_{eff} in the SER, a larger number of solitons is needed, which is consistent with Eq. (3).

In conclusion, we show DSG in SiN microresonators both numerically and experimentally. We find with certain thermal strength the solitons either annihilate or survive in different experimental runs, with annihilation or survival strongly correlated to the number of solitons generated at the end of the laser scan. The presence of TO chaos allows various routes to soliton formation, including delayed spontaneous soliton generation from the chaotic state. The spontaneous soliton generation enables soliton generation with a slow tuning speed and suggests that rapid and precise control of the laser tuning is not necessarily required. Our findings suggest that DSG can be facilitated if thermal effects can be lowered.

Funding. Air Force Office of Scientific Research (AFOSR) (FA9550-15-1-0211); Defense Advanced Research Projects Agency (DARPA) (W31P40-13-1-0018); National Science Foundation (NSF) (ECCS-1509578).

REFERENCES

1. P. Del'Haye, A. Schliesser, O. Arcizet, T. Wilken, R. Holzwarth, and T. J. Kippenberg, Nature **450**, 1214 (2007).
2. T. Kippenberg, R. Holzwarth, and S. Diddams, Science **332**, 555 (2011).
3. A. B. Matsko, W. Liang, A. A. Savchenkov, and L. Maleki, Opt. Lett. **38**, 525 (2013).
4. T. Herr, V. Brasch, J. D. Jost, C. Y. Wang, N. M. Kondratiev, M. L. Gorodetsky, and T. J. Kippenberg, Nat. Photonics **8**, 145 (2014).
5. S. Coen and M. Erkintalo, Opt. Lett. **38**, 1790 (2013).
6. C. Bao and C. Yang, Phys. Rev. A **92**, 053831 (2015).
7. V. Brasch, M. Geiselmann, T. Herr, G. Lihachev, M. Pfeiffer, M. Gorodetsky, and T. Kippenberg, Science **351**, 357 (2016).
8. P.-H. Wang, J. A. Jaramillo-Villegas, Y. Xuan, X. Xue, C. Bao, D. E. Leaird, M. Qi, and A. M. Weiner, Opt. Express **24**, 10890 (2016).
9. X. Yi, Q.-F. Yang, K. Y. Yang, M.-G. Suh, and K. Vahala, Optica **2**, 1078 (2015).
10. V. Brasch, M. Geiselmann, M. H. P. Pfeiffer, and T. J. Kippenberg, Opt. Express **24**, 29312 (2016).
11. H. Guo, M. Karpov, E. Lucas, A. Kordts, M. H. P. Pfeiffer, V. Brasch, G. Lihachev, V. E. Lobanov, M. L. Gorodetsky, and T. J. Kippenberg, Nat. Phys. **13**, 94 (2017).
12. C. Joshi, J. K. Jang, K. Luke, X. Ji, S. A. Miller, A. Klenner, Y. Okawachi, M. Lipson, and A. L. Gaeta, Opt. Lett. **41**, 2565 (2016).
13. M. Yu, Y. Okawachi, A. G. Griffith, M. Lipson, and A. L. Gaeta, Optica **3**, 854 (2016).
14. Q. Li, T. C. Briles, D. A. Westly, T. E. Drake, J. R. Stone, B. R. Ilic, S. A. Diddams, S. B. Papp, and K. Srinivasan, Optica **4**, 193 (2017).
15. J. Pfeifle, V. Brasch, M. Lauermann, Y. Yu, D. Wegner, T. Herr, K. Hartinger, P. Schindler, J. Li, D. Hillerkuss, R. Schmogrow, C. Weimann, R. Holzwarth, W. Freude, J. Leuthold, T. Kippenberg, and C. Koos, Nat. Photonics **8**, 375 (2014).
16. M.-G. Suh, Q.-F. Yang, K. Y. Yang, X. Yi, and K. J. Vahala, Science **354**, 600 (2016).
17. F. Ferdous, H. Miao, D. E. Leaird, K. Srinivasan, J. Wang, L. Chen, L. T. Varghese, and A. M. Weiner, Nat. Photonics **5**, 770 (2011).
18. S. Coen, H. G. Randle, T. Sylvestre, and M. Erkintalo, Opt. Lett. **38**, 37 (2013).
19. C. Bao, J. A. Jaramillo-Villegas, Y. Xuan, D. E. Leaird, M. Qi, and A. M. Weiner, Phys. Rev. Lett. **117**, 163901 (2016).
20. J. Wang, Y. Xuan, A. M. Weiner, and M. Qi, *Conference on Lasers and Electro-Optic* (Optical Society of America, 2014), paper STh1M.8.
21. M. Karpov, H. Guo, A. Kordts, V. Brasch, M. H. Pfeiffer, M. Zervas, M. Geiselmann, and T. J. Kippenberg, Phys. Rev. Lett. **116**, 103902 (2016).